Journal of Alloys and Compounds 516 (2012) 102–106

Contents lists available at SciVerse ScienceDirect

Journal of Alloys and Compounds

journal homepage: www.elsevier.com/locate/jallcom

Robust ultra-thin RuMo alloy film as a seedless Cu diffusion barrier

Kuo-Chung Hsu [a], Dung-Ching Perng [a,b,*], Yi-Chun Wang [a]

[a] Institute of Microelectronics and Department of Electrical Engineering, National Cheng Kung University, Tainan 701, Taiwan
[b] Center for Micro/Nano Science and Technology, National Cheng Kung University, Tainan 701, Taiwan

ARTICLE INFO

Article history:
Received 15 August 2011
Received in revised form
15 November 2011
Accepted 29 November 2011
Available online 8 December 2011

Keywords:
RuMo alloy
Cu diffusion barrier
Cu metallization

ABSTRACT

This study investigated the properties of 5 nm-thick RuMo film as a Cu diffusion barrier. The sheet resistance variation and X-ray diffraction patterns show that the RuMo alloy film has excellent barrier performance and that it is stable upon annealing at 725 °C against Cu. The transmission electron microscopy micrograph and diffraction patterns show that the RuMo film is an amorphous-like structure, whereas pure Ru film is a nano-crystalline structure. The elements' depth profiles, analyzed by X-ray photoelectron spectroscopy, indicate no inter-diffusion behavior between the Cu and Si layer, even annealing at 700 °C. Lower leakage current has been achieved from the Cu/barrier/insulator/Si test structure using RuMo film as the barrier layer. A 5 nm ultrathin RuMo film provided two orders of magnitude improvement in leakage current and also exhibited a 175 °C improvement in thermal stability than that of the pure Ru film. It is a potential candidate as a seedless Cu diffusion barrier for advanced Cu interconnects.

1. Introduction

With continuing shrinkage of integrated circuit (IC) dimensions, the resistance–capacitance time delay (*R–C* delay) of the back end of line (BEoL) interconnection became a major contribution to the total time delay in integrated circuits (ICs) [1,2]. Replacing traditional Al and dense oxide with Cu and porous low k material has been successfully integrated in advanced metallization for a lower *R–C* delay time [3]. However, Cu has a higher diffusion coefficient in the dielectric and reacts easily with Si at temperatures above 300 °C [4], which could cause early failure of the integrated circuits. Therefore, a liner as a diffusion barrier, inserted between Cu and the dielectric, is necessary for effectively halting Cu penetration into the dielectric.

Ta/TaN is a commonly used Cu diffusion barrier due to its insolubility in Cu and high barrier capability against Cu diffusion [5,6]. Unfortunately, in the more advanced IC generations, such as sub-32 nm technology, a thinner barrier is necessary, because the volume ratio of the diffusion barrier to the whole conducting line will be too high if barrier thickness is not scaled down accordingly. However, thinning Ta/TaN layer, which exhibits high resistivity, cannot meet the requirement for more advanced Cu metallization [7].

Ruthenium, a transitional metal, has a bulk electrical resistivity of 7.1 μΩ-cm that is lower than that of Ta (13.6 μΩ-cm). The Ru–Cu phase diagram shows negligible solid solubility between the elements [8]. Moreover, Ru can directly plate a Cu film without a Cu seed layer, which reduces a process step. The process also relax seed/barrier combined thickness requirement and is an attractive integrated process [9]. Therefore, pure Ru film has been investigated as a potential candidate for a seedless Cu diffusion barrier for future generations [10,11]. However, pure Ru film exhibits a columnar grain structure; the vertical grain boundaries provide Cu with the high diffusion paths, which lead to early failure of the Ru barrier [11]. Recently, the improvement of Ru barrier-performance against Cu has been widely studied [12–14]. Adding extra elements, such as N, P, and Ta as impurities in the lattice matrix of Ru film is a way to enhance Cu diffusion barrier properties [12,14,15]. Damayanti et al. indicated that the dissolved N in Ru film can modify crystalline Ru film trending to an amorphous microstructure [12]. The elements added into Ru film could not only be stuffed at the grain boundaries but also alter the microstructure or amorphize the Ru film. As a result, it can obviously improve barrier performance against Cu diffusion.

Mo shows no solid solutions with Cu [16]; it has a lower bulk resistivity of only 5.18 μΩ-cm and has a high melting point (melting point of Mo is 2623 °C). Mo film as a barrier layer also exhibits a good electromigration performance [17]. In this study, a small amount of Mo was added to the Ru film and RuMo alloy film as a Cu diffusion barrier has been investigated. The film properties of RuMo alloy film, including its thermal stability, Cu diffusion barrier performance, and film micro-structure are discussed.

* Corresponding author at: Institute of Microelectronics and Department of Electrical Engineering, National Cheng Kung University, One University Road, Tainan 701, Taiwan. Tel.: +886 6 275 7575x62433; fax: +886 6 234 5482.
E-mail address: dcperng@ee.ncku.edu.tw (D.-C. Perng).

0925-8388/$ – see front matter © 2011 Elsevier B.V. All rights reserved.
doi:10.1016/j.jallcom.2011.11.144

Table 1
The atomic compositions, sputtering conditions and failure temperatures of RuMo alloy and pure Ru films. Film composition was measured by XPS.

Films	Sputter conditions		Composition			Failure temperature (°C)
	Ru target power (W) by DC power	Mo target power (W) by RF power	Ru (at.%)	Mo (at.%)	O (at.%)	
Ru	40	–	92.6	–	7.4	575
RuMo I	40	10	92.8	3.1	4.1	750
RuMo II	40	40	33.9	46.3	19.8	600

2. Experimental

A 4-in. p-type Si wafer was used as substrate. Before the barrier and Cu film deposition, the Si substrate was cleaned by diluted buffered HF solution. Next, a 5 nm thick RuMo film is deposited on the Si substrate by a three-gun co-sputtering system, with a working pressure of 1.2×10^{-2} Torr and a 99.9995% purity level of Ar gas flow at 8 sccm. The base pressure of the sputter chamber is below 1×10^{-5} Torr. The sputtering power of the Ru target was set to direct current (DC) 40 W, whereas the power of the Mo target was varied from 10 to 40 W with radio frequency (RF) to adjust the composition of the RuMo films. All target diameters were 2 in. and purities were above 99.95%. A 100 nm thick Cu film is then deposited in situ on the 5 nm RuMo film/Si substrate by DC power at 80 W. To evaluate the microstructure of the barrier films, the 5 nm thick RuMo and Ru films are deposited separately on Si substrates for further analysis. Microstructure and thermal stability of the studied films were evaluated by thermal annealing using a rapid thermal annealing (RTA) system (ULVAC, model: MILA-5000) in a vacuum level of 1×10^{-5} Torr. The four-point probe instrument was used to measure sheet resistance variation. The gazing incident of X-ray diffractometer (GIXRD, Rigaku, D/MAX2500) with a CuKα (λ = 0.15406 nm) radiation source was applied to analyze the film's microstructure and phase transformation. The X-ray photoelectron spectroscopy (XPS, PHI 5000 VersaProbe) was employed to analyze atomic composition and the depth profile for Ru and RuMo film. The high resolution transitional electron microscopy (HRTEM, JEOL, JEM-2100F) was used to observe microstructure and thickness of barrier films. The Cu/barrier/TEOS/Si stacked films, as a metal-isolator-semiconductor (MIS) structure, were used for the measurements of leakage current densities with a Keithley 2400.

3. Results and discussion

Barrier performance of the 5 nm-thick RuMo and pure Ru film were preliminarily evaluated by thermal annealing using a Cu/barrier/Si structure. The atomic compositions and failure temperature of the barrier films are summarized in Table 1. The atomic composition of Ru and RuMo alloy films were evaluated by XPS analyses and the failure temperature was defined as the annealing temperature that its sheet resistance increased by at least one order of magnitude. The oxygen content in the barrier films are possibly resulted from the residual oxygen of the process chamber. The higher oxygen content of the RuMo II film could be attributed to the high oxygen affinity of Mo [18]. The RuMo film with lower Mo content (RuMo I) exhibits the best thermal stability. Therefore, the RuMo I film (the acronym RuMo will be used hereafter) was chosen for further investigations.

Fig. 1 shows the sheet resistance variations of the as-deposited and post-annealed Cu/Ru/Si and Cu/RuMo/Si structures. Both sheet resistances decrease initially with an increasing annealing temperature up to 500 °C. The decrease in resistances could be ascribed to grain growth and decreasing defect density of Cu film [19,20]. For the Cu/5 nm Ru/Si sample, the increase of sheet resistance starts after annealing at 550 °C, and it increases acutely after annealing at 575 °C. The obvious increase of sheet resistance could be considered the signature of Cu_3Si formation [21]. The forming of Cu_3Si is caused by failure of the Ru barrier. In contrast, the sheet resistance of the Cu/RuMo/Si stacked films maintains a low value even after a 700 °C anneal, indicating that the 5 nm RuMo film reveals high thermal stability. By further increasing the annealing temperature, the sheet resistance drastically increases at 750 °C anneal. However, the 5 nm RuMo film demonstrated a higher thermal stability than that of pure Ru against Cu diffusion by about 175 °C.

The XRD patterns of Cu/Ru/Si and Cu/RuMo/Si structures with and without annealing are shown in Fig. 2a and b, respectively. The 2θ diffraction peaks found at 43.3°, 50.6° and 74.3° correspond to Cu(1 1 1), Cu(2 0 0) and Cu(2 2 0), respectively. The peaks of Cu become sharper with elevated annealing temperature. This sharpening of Cu peaks can be ascribed to the grain growth of the Cu film, which is in agreement with descended sheet resistance of the annealed Cu/barrier/Si (Fig. 1) [22]. Fig. 2a presents the XRD spectra of the Cu/Ru/Si structure with various annealing temperatures. No obvious peak besides Cu can be observed before 550 °C annealing; it suggests that the 5 nm Ru film is stable up to 550 °C. However, small Cu_3Si peak appeared after annealing at 575 °C, and then becomes visibly sharper. No Cu peak can be observed after annealing at 600 °C. The appearance of Cu_3Si suggests that an interaction of Cu and Si occurred in Cu/Ru/Si stacked films, and the Ru barrier fails to block Cu diffusion effectively. The results also agree with the finding of sharply raised sheet resistance (Fig. 1). In comparison, the XRD spectra of Cu/RuMo/Si samples with various annealing temperatures are shown in Fig. 2b. No obvious Cu_3Si diffraction peak can be detected even after annealing at 725 °C. It suggests that the 5 nm RuMo alloy film can effectively block Cu diffusion and therefore prevent the reaction between Cu and Si at 725 °C. After annealing at 750 °C, the absence of Cu peaks and the appearance of Cu_3Si peaks suggest that massive Cu atoms penetrate through the RuMo layer and react with Si. Nonetheless, the 5 nm RuMo layer can prohibit massive diffusion of Cu into the Si substrate up to 725 °C, and with an improvement of more than 175 °C in thermal stability over a pure Ru film.

Further investigations of the film's properties of pure Ru and the RuMo film deposited on Si were performed by GIXRD without Cu capping. The diffraction patterns of pure Ru and RuMo film after various annealing are shown in Fig. 3a and b, respectively. The 2θ values at 38.385, 42.19 and 44.021° correspond to Ru(1 0 0), Ru(0 0 2) and Ru(1 0 1) peaks, respectively. In Fig. 3a, small but present Ru peaks of the as-deposited sample suggest that the as-deposited Ru film is a nano-crystalline structure. The Ru peaks drastically increase when the annealing temperature is elevated to 550 °C, which can be contributed to grains growth and re-crystallization of the Ru film. The grain boundaries in the

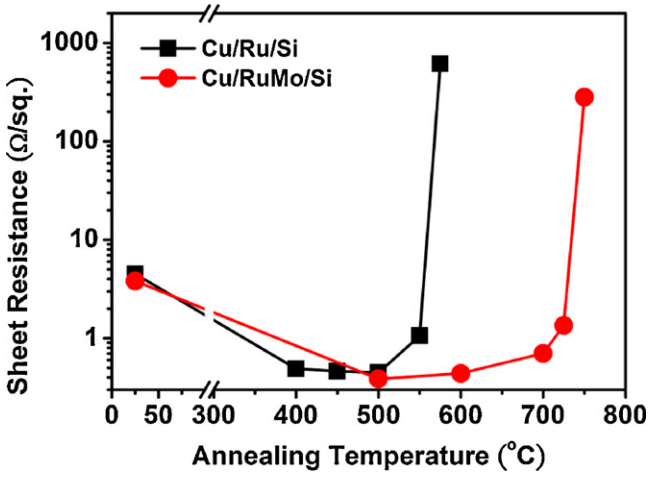

Fig. 1. Sheet resistances of the Cu/5 nm barrier/Si structures after annealing at various temperatures.

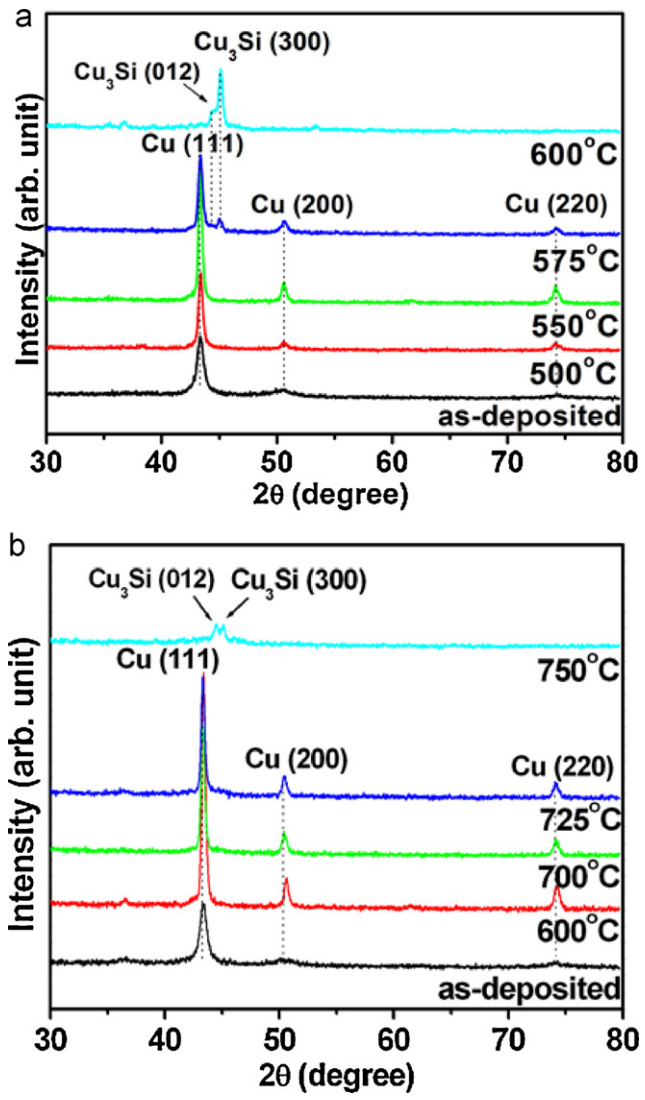

Fig. 2. X-ray diffraction spectra of the (a) Cu/5 nm Ru/Si and (b) Cu/5 nm RuMo/Si stacked film annealing at various temperatures.

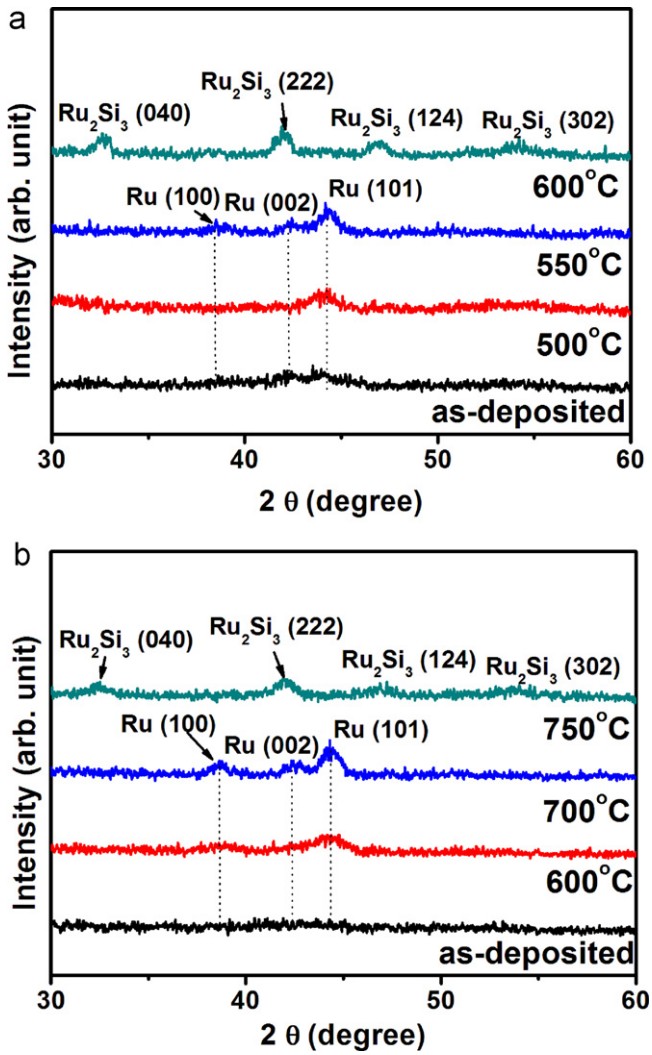

Fig. 3. XRD patterns of the 5 nm-thick (a) pure Ru and (b) RuMo deposited on a Si substrate with various annealing temperatures.

nano-crystalline Ru film provide many fast diffusion paths for Cu to penetrate the barrier layer, which significantly degrade the barrier performance. Furthermore, after annealing at 600 °C, the Ru_2Si_3 peaks emerge and can be clearly observed in the XRD spectra. The formation of Ru_2Si_3 suggests that the Ru film reacts with the underlying Si layer during the annealing. Arunagiri et al. [10] indicated that the poor barrier performance of pure Ru is attributed to its columnar microstructure for the as-deposited film and the low activation energy of forming Ru_2Si_3 upon annealing. The relatively denser Ru film could transform to a less dense Ru_2Si_3 with thermal annealing [23]. The less dense Ru_2Si_3 structure provides rough interface and even faster diffusion paths to accelerate copper's penetration [10,24,25].

In comparison, no obvious peak can be observed in Fig. 3b for the as-deposited RuMo film. It implies that the as-deposited RuMo film could be an amorphous-like microstructure. Even after annealing at 600 °C, only weak, broad Ru peaks can be detected. A non-obvious Ru peak suggests that the RuMo film likely remains as an amorphous-like microstructure. A barrier lack of grain boundaries means that there is less easy diffusion path for Cu to penetrate. As the annealing temperature raises to 700 °C, the Ru peaks emerge, which implies that Ru in the RuMo film starts to re-crystallize. At this annealing temperature, no Ru_2Si_3 peak exists, suggesting that the RuMo alloy is more thermally stable than the pure Ru film. The significant improvement in Cu barrier performance of the RuMo film is mainly attributed to the amorphous-like microstructure. The added Mo disturbed or hindered the ability of Ru to form a nanocrystalline structure in the RuMo film. As the annealing temperature raise to 750 °C, weak Ru_2Si_3 peaks and no Ru peak were found, implies that an interaction between Ru and Si has occurred.

The inter-diffusion behavior of each layer was observed by the XPS depth profiling after annealing. Fig. 4a shows the element's depth profiles of the post 600 °C annealed Cu/RuMo/Si sample. The Cu signal drops imminently before the RuMo layer and no Cu signal appears in the Si layer. Those individual instances, with clear interfacial layers, suggest that RuMo film blocks the diffusion of Cu into the Si layer. After annealing at 700 °C (Fig. 4b), the signal of Ru becomes broader, indicating that Ru tends to diffuse into the Cu and Si layers at higher annealing temperature. However, Cu signal is not present in the Si layer suggests that the RuMo film can effectively block mass Cu penetration into Si at 700 °C. Fig. 4c shows the 600 °C post-annealed Cu/Ru/Si structure, where no interface can be recognized from the Cu/Ru/Si stacked layers. The Cu atoms penetrate through the pure Ru barrier and deeply diffuse into the Si layer. Obviously, the inter-diffusion between Cu and Si indicates that the pure Ru film failed as a barrier against Cu

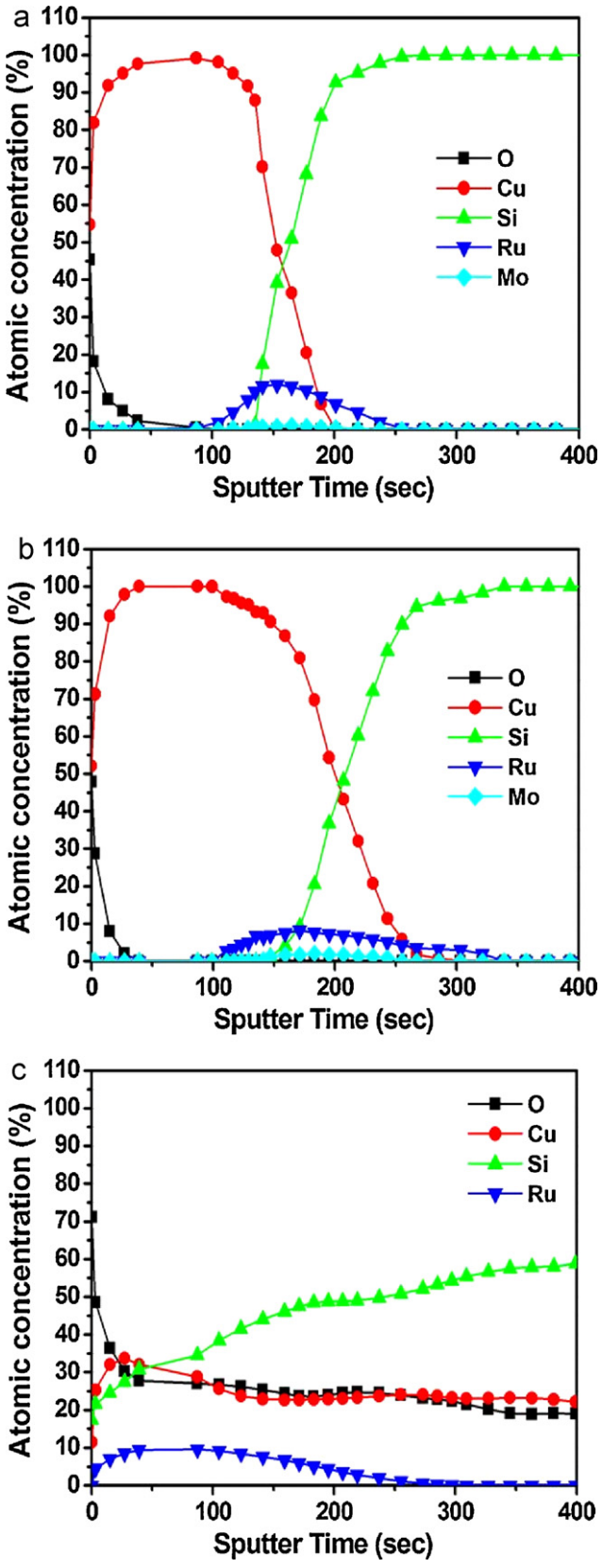

Fig. 4. XPS depth profiling of (a) the Cu/RuMo/Si stacked films after annealing at 600 °C and (b) the Cu/RuMo/Si stacked films after annealing at 700 °C and (c) the Cu/Ru/Si stacked films after annealing at 600 °C. All barrier films are 5 nm thick.

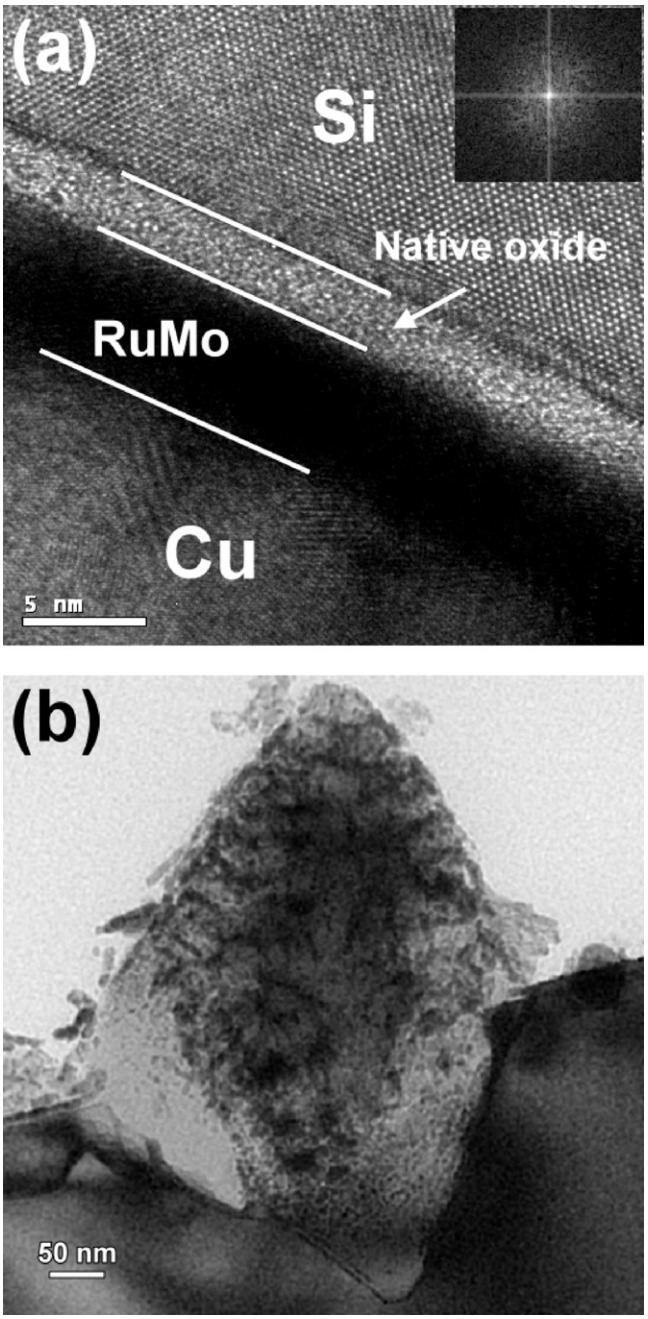

Fig. 5. The cross-sectional TEM micrograph of (a) Cu/RuMo/Si stacked films, the inserted image is FTED patterns of RuMo layer, and (b) Cu/Ru/Si stacked films. Both samples received 1 min of 600 °C annealing.

diffusion at an annealing temperature of 600 °C. The Cu could diffuse into Si via grain boundaries of the Ru layer. Unlike Ru, lack of grain boundaries of the RuMo film can impressively enhance barrier performance against Cu diffusion, even at an annealing temperature of 700 °C. An obvious improvement of thermal stability was obtained by adding a small amount of Mo to the Ru film. Cu can be easily oxidized at atmosphere. The XPS depth profiles of all samples in Fig. 4 indicate similar amount of oxygen content at surfaces (~45 at.%). The high oxygen content at all sample's surfaces could be caused by exposure of samples in air before the analyses [26–28]. Based on (a) all samples have native Cu oxide(s) formed at the surfaces, (b) the sheet resistance (Fig. 1) of 600 °C annealed Cu/Ru/Si sample is approximately two-order of magnitudes higher than that of Cu/RuMo/Si sample, and (c) Cu_3Si was formed at 600 °C

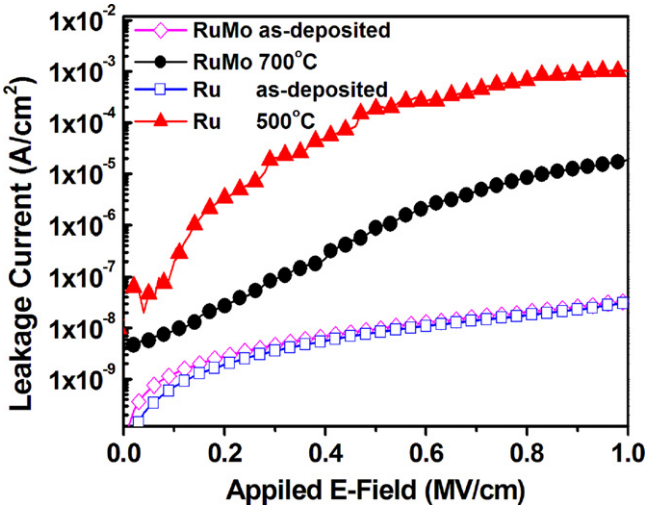

Fig. 6. Leakage current densities of the Cu/barrier/TEOS/Si structures as-deposited and after a 1-min annealing at 500 °C and 700 °C.

for Cu/Ru/Si sample (Fig. 2a). Therefore, the formation of Cu_3Si should be the root cause responsible for the increasing in film resistivity and the surface native Cu oxide has no significant contribution to overall film's resistivity.

Fig. 5a and b shows the cross-sectional micrographs of the stacked Cu/RuMo/Si and Cu/Ru/Si structures that have undergone annealing at 600 °C, respectively. Fig. 5a indicates the RuMo barrier layer is about 5 nm thick, and ~2 nm thick native oxide remains at the interface between RuMo and Si layers. The insert image shows Fourier transformed electron diffraction (FTED) patterns from the TEM image of the RuMo film. The FTED image suggests that the 5 nm RuMo film is a non-crystalline microstructure even after 600 °C annealing, which agrees with the lack of clear diffraction peak shown in Fig. 3b. Moreover, the RuMo layer exhibits uniformly and has a clear interface between Cu and Si after annealing at 600 °C. This further confirms that the 5 nm RuMo film is a good Cu barrier with high thermal stability. Fig. 5b shows the cross-sectional TEM micrograph of the Cu/Ru/Si structure after annealing at 600 °C. A distinct triangular structure was found. According to the XRD patterns (Fig. 2a) and acutely ascendant sheet resistance (Fig. 1), this triangular film could be considered as part of the formation of Cu_3Si [29,30]. The forming Cu_3Si in the Cu/Ru/Si stacked films implies that Cu atoms already penetrated through the Ru barrier and reacted with Si. In contrast, the 5 nm RuMo film is intact and reveals a robust Cu diffusion barrier.

The leakage currents were evaluated by the Cu/5 nm barrier/TEOS/Si MIS structure. The results are shown in Fig. 6. The sample with a pure Ru barrier exhibits a high leakage current after annealing at 600 °C. The high leakage current of the Ru sample after annealing is attributed to the out-diffusion of Cu into the dielectric film through a poor Ru barrier layer [31]. The leakage current measured from the 5 nm RuMo barrier sample is two orders of magnitude lower than that of the pure 5 nm Ru sample, even with a higher annealing temperature at 700 °C. The low leakage current density suggests that the RuMo film is a good candidate as a diffusion barrier against Cu.

4. Conclusions

A distinguished Cu barrier performance of a 5 nm-thick RuMo film has been demonstrated. The results of sheet resistance, GIXRD, XPS element's depth profiles and TEM micrograph indicate that a 5 nm-thick RuMo film is thermally stable up to 725 °C. Whereas, the Cu barrier function of a pure Ru film fails at a lower annealing temperature of 575 °C. Small amounts of Mo added into the Ru film can drastically improve the barrier performance by about 175 °C. The diffraction patterns of post-annealed RuMo film suggest that RuMo film preserves its amorphous-like microstructure after 600 °C annealing. The inter-diffusion behaviors between Cu and Si can be delayed to beyond 700 °C by inserting an ultrathin 5 nm RuMo barrier in between. The TEM micrograph shows that the 5 nm RuMo film reveals a uniform and glassy-like microstructure after being annealed at 600 °C, which suggests that the 5 nm RuMo film is a robust Cu barrier. The leakage current density of a MIS structure using a 5 nm RuMo barrier film shows an improvement of more than two orders of magnitude over that of pure Ru film. The RuMo film could be a potential seedless Cu diffusion barrier for advanced Cu metallization.

Acknowledgements

The authors would like to thank the CRD thin film group of United Microelectronic Co. for TEOS film deposition. The funding support of the National Science Council of Taiwan under contract no. NSC 99-2221-E-006-138 is acknowledged.

References

[1] M.T. Bohr, Solid State Technol. 39 (1996) 105–111.
[2] S. Bothra, B. Rogers, M. Kellam, C.M. Osburn, IEEE Trans. Electron Dev. 40 (1993) 591–597.
[3] A.E. Kaloyeros, E. Eisenbraun, Annu. Rev. Mater. Res. 30 (2000) 363–385.
[4] C.-A. Chang, J. Appl. Phys. 67 (1990) 566–569.
[5] T. Oku, E. Kawakami, M. Uekubo, K. Takahiro, S. Yamaguchi, M. Murakami, Appl. Surf. Sci. 99 (1996) 265–272.
[6] Q. Xie, X.P. Qu, J.J. Tan, Y.L. Jiang, M. Zhou, T. Chen, G.P. Ru, Appl. Surf. Sci. 253 (2006) 1666–1672.
[7] M.H. Tsai, S.C. Sun, C.E. Tsai, S.H. Chuang, H.T. Chiu, J. Appl. Phys. 79 (1996) 6932–6938.
[8] H. Okamoto, J. Phase Equilib. 13 (1992) 440.
[9] O. Chyan, T.N. Arunagiri, T. Ponnuswamy, J. Electrochem. Soc. 150 (2003) C347–C350.
[10] T.N. Arunagiri, Y. Zhang, O. Chyan, M. El-Bouanani, M.J. Kim, K.H. Chen, C.T. Wu, L.C. Chen, Appl. Phys. Lett. 86 (2005) 083104.
[11] R. Chan, T.N. Arunagiri, Y. Zhang, a O. Chyan, R.M. Wallace, M.J. Kim, T.Q. Hurd, Electrochem, Solid State Lett. 7 (2004) G154–G157.
[12] M. Damayanti, T. Sritharan, S.G. Mhaisalkar, H.J. Engelmann, E. Zschech, A.V. Vairagar, L. Chan, Electrochem. Solid State Lett. 10 (2007) P15–P17.
[13] C.X. Yang, S.J. Ding, D.W. Zhang, P.F. Wang, X.P. Qu, R. Liu, Electrochem. Solid State Lett. 14 (2011) H84–H87.
[14] D.C. Perng, J.B. Yeh, K.C. Hsu, Appl. Surf. Sci. 254 (2008) 6059–6062.
[15] C.W. Chen, J.S. Chen, J.S. Jeng, J. Electrochem. Soc. 155 (2008) H1003–H1008.
[16] P.R. Subramanlan, D.E. Laughlin, J. Phase Equilib. 11 (1990) 169–172.
[17] D.S. Gardner, J. Onuki, K. Kudoo, Y. Misawa, Q.T. Vu, Thin Solid Films 262 (1995) 104–119.
[18] M. Kitada, N. Shimizu, J. Mater. Sci. 19 (1984) 1339–1342.
[19] K.H. Min, K.C. Chun, K.B. Kim, J. Vac. Sci. Technol. B 14 (1996) 3263–3269.
[20] Y. Wang, F. Cao, Z. Song, C.H. Zhao, Electrochem. Solid State Lett. 10 (2007) H299–H301.
[21] S. Song, Y. Liu, M. Li, D. Mao, C. Chang, H. Ling, Microelectron. Eng. 83 (2006) 423–427.
[22] M.B. Takeyama, T. Itoi, E. Aoyagi, A. Noya, Appl. Surf. Sci. 190 (2002) 450–454.
[23] Y. Matsui, Y. Nakamura, Y. Shimamoto, M. Hiratani, Thin Solid Films 437 (2003) 51–56.
[24] M. Damayanti, T. Sritharan, S.G. Mhaisalkar, E. Phoon, L. Chan, J. Mater. Res. 22 (2007) 2505–2511.
[25] J.J. Tan, X.P. Qu, Q. Xie, Y. Zhou, G.P. Ru, Thin Solid Films 504 (2006) 231–234.
[26] J.W. Lim, J. Iijima, Y. Zhu, J.H. Yoo, G.S. Choi, K. Mimura, M. Isshiki, Thin Solid Films 516 (2008) 4040–4046.
[27] J. Iijima, J.W. Lim, S.H. Hong, S. Suzuki, K. Mimura, M. Isshiki, Appl. Surf. Sci. 253 (2006) 2825–2829.
[28] S.H. Kim, H.T. Kim, S.S. Yim, D.J. Lee, K.S. Kim, H.M. Kim, K.B. Kim, H. Sohn, J. Electrochem. Soc. 155 (2008) H589–H594.
[29] Y.L. Kuo, C. Lee, J.C. Lin, Y.W. Yen, W.H. Lee, Thin Solid Films 484 (2005) 265–271.
[30] P. Majumder, C. Takoudis, Nanotechnology 19 (2008) 205202.
[31] A.A. Istratov, E.R. Weber, J. Electrochem. Soc. 149 (2002) G21–G30.